Vol. 90 No. 6 pp. 2022–2035 ACTA GEOLOGICA SINICA (English Edition) Dec. 2016

In Situ Stress Measurements in the Lhasa Terrane, Tibetan Plateau, China

MENG Wen[1, 2], GUO Changbao[1, 2, *], ZHANG Yongshuang[1, 2], DU Yuben[3], ZHANG Min[3], BAO Linhai[4] and ZHANG Peng[1, 2]

1 *Institute of Geomechanics, Chinese Academy of Geological Sciences, Beijing 100081, China*
2 *Key Laboratory of Neotectonic Movement and Geohazard, Ministry of Land and Resourses, Beijing 100081, China;*
3 *China Railway Eryuan Engineering Group CO.LTD, Sichuan 610031, China*
4 *The Institute of Crustal Dynamics, China Earthquake Administration, Beijing 100085, China*

Abstract: Tectonic activities are frequent in the Lhasa terrane because of the ongoing collision between the India and Eurasia plates. Knowledge of the stress state is critical to evaluate the crustal stability and the design of underground excavations. Because of the limitations imposed by natural conditions, little research has been performed on the present crustal in situ stress in the Tibetan Plateau, and further study is imperative. In this study, hydraulic fracturing measurements were conducted in Nyching County (LZX) and Lang County (LX), Lhasa terrane to characterize the shallow crustal stress state. The results indicate that the stress state in the LZX borehole is markedly different from that in the LX borehole, in both magnitude and orientation. At the same measurement depths, the magnitudes of horizontal principal stresses in the LX borehole are 1.5–3.0 times larger than those in the LZX borehole. The stress regime in the LX borehole favors reverse faulting characterized by $S_H>S_h>S_v$, where S_H, S_h, and S_v are maximum horizontal, minimum horizontal, and vertical principal stresses, respectively. The S_H and S_h values are approximately three and two times greater than S_v. Fracture impression results reveal that S_H in the LX borehole are predominantly N–S, while in the LZX borehole the maximum horizontal principal stress is mainly in the NNE-direction. The heterogeneity of the regional stress state might be a result of the population and distribution of local structures and seismic activities. The stress state in the LX borehole has exceeded the critical state of failure equilibrium, and there is an optimally orientated pre-existing fault near the borehole. It can be concluded that the optimally orientated fault is likely to be active when the stress has built up sufficiently to destroy the frictional equilibrium; it is suggested that research focus should be placed on this in future. The stress states in boreholes LZX and LX indicate uniformity of the regional stress field and diversity of the local stress fields resulting from the interactions among regional dynamic forces, tectonic stress field, and geological structures.

Key words: in situ stress, hydraulic fracturing, Lhasa terrane

1 Introduction

Knowledge of the present-day crustal stress state provides information on the regional tectonic setting as well as the small-scale structural characteristics (Zoback, 1992; Chang et al., 2010). Exploration of the crustal stress state and its characteristics is critical for understanding the physical processes inside the crust and fault activity (Li, 1973) because tectonic activities and the resulting geological disasters are closely related to the crustal tectonic stress state. Furthermore, knowledge of the crustal stress state is critical to obtain the stress information for the design of underground excavations such as mining, tunnels, and nuclear waste disposal, and therefore, stress measurements are routinely conducted prior to the commencement of engineering projects (Wu et al., 2009; Chen et al., 2012; Meng et al., 2012, 2015; Zhao et al., 2013; Tan et al., 2015; Sun et al., 2015).

Significant focus has been placed on the Tibetan Plateau because of its intensive tectonic activities resulting from the ongoing continental collision between the India and

* Corresponding author. E-mail: guochangbao@cags.ac.cn

Eurasia plates (Zhang et al., 2015). Furthermore, major engineering projects such as large-scale water conservancy and hydropower projects, the Sichuan–Tibet railway, and the Lhasa–Nyching highway are planned. It is imperative to characterize the in situ stress state to provide fundamental data for further analysis. However, previous research on the stress state has mainly focused on inversion interpretation based on earthquake focal mechanisms, fault plane solutions, and numerical simulations (Xu, 2002; Zhu and Shi, 2005; Xu and Zhao, 2006; Xie et al., 2004, 2015), but not direct in situ measurements. Borehole field-test methods, such as hydraulic fracturing, which has been widely used to measure the stress state at shallow to great depths because of its practicality and reliability, can determine the in situ stress directly. Successful hydraulic fracturing measurements generally provide an estimate of the in situ principal stress, including both the magnitude and direction.

In the present study, hydraulic fracturing was conducted in Nyching County (LZX) and Lang County (LX), of the Lhasa terrane, and in situ stress measurement results were used to characterize the present-day stress state and gain an insight into the regional stress field in the Lhasa terrane. The relationships among the in situ stress fields, geological structures, and regional dynamic forces in the Lhasa terrane are described. Furthermore, the implications of the in situ stress in terms of the stress magnitude and orientation are discussed for fault activity. The results provide the fundamental data and knowledge on geodynamic and crustal stability, and have significant implications for future engineering construction.

2 Tectonic Setting

The Tibetan Plateau is a typical example of continuing collision tectonics (Dai et al., 2014; Wu et al., 2014). After the collision between the India and Eurasia plates at 70–50 Ma, which created the Himalayan orogen, the India plate has continued to move northward to the Eurasia plate at a rate of approximately 40–50 mm/year (Yin and Harrison, 2000; USGS, 2013; Harris, 2007). The 2000-km-long, east–west-trending Himalayan orogenic belt terminates at two Himalayan syntaxes in the east and west. In contrast to the dominantly dip-slip faulting along the Himalayan orogen, strike-slip tectonics prevail in the eastern and western Himalayan syntaxes (Burg et al., 1998; Wang et al., 2001; Ding et al., 2001). In the eastern Himalayan syntaxis, the main tectonic units are the Himalaya, Lhasa, and Qiangtang terranes (Fig. 1). The Lhasa terrane in southern Tibet is generally accepted to have been the last crustal block to have accreted with Eurasia prior to its collision with the northward-drifting Indian continent during the Cenozoicera (Dong et al., 2013). The rock basement in the Lhasa terrane is mainly Proterozoic metamorphic rock and the sedimentary cover is composed of Paleozoic, Mesozoic, and a small account of Cenozoicstrata (Wang et al., 2001). The Yarlung Zangbo and Bangong–Nujiang suture zones form the southern and northern boundaries of the Lhasa terrane. The Yarlung Zangbo suture zone, which is mainly composed of ophiolite melange, formed as a result of compression from continental collision and orogenic movement (Liu et al., 2000).

The major faults in the study area are the Nujiang, Jiali, Yarlung Zangbo, Zhamu–Maniwen, and Apalong faults. GPS data indicate that the Yarlung Zangbo fault shows dextral-slip movement with slip rates near the eastern Himalayan syntaxis that are much higher than those in the western section (Tang et al., 2010). The Jiali fault shows dextral-slip movement to the west of the eastern Himalayan syntaxis and sinistral-slip movement to the east of the eastern Himalayan syntaxis. Although fault activity is relatively weak overall, local sections adjacent to extensional basins show higher movement rate (Ren et al., 2000; Tang et al., 2010). The Nujiang fault is characterized by compressional and dextral-slip movements to the west and east of the eastern Himalayan syntaxis, respectively (Tang et al., 2010). The NE-striking Zhamu–Maniwen fault, with a total length of 140 km (He et al., 2005), has experienced several *M* 5–5.9 earthquakes. The Apalong fault trends at approximately N60°W, and shows a combination of thrust and dextral-slip movements. This fault is related to the 1950 *M* 8.6 Motuo–Zayu earthquake (Song et al., 2011).

As the leading affected zone of continent–continent collision, strong earthquake activities are characteristic of the south of the Tibetan Plateau. More strong earthquakes are likely to occur in future, as determined from analysis of the correlativity between global and regional earthquake activities, the temporal and spatial distributions of earthquakes, and the great earthquakes-rupture features in the Tibetan Plateau (Bilham et al., 2001; Deng et al., 2014). Fig. 1 shows the historic earthquakes in the eastern Himalayan syntaxis and its neighborhood regions. These events show spatial heterogeneity in that they are concentrated along faults, particularly where faults converge and cross, indicating the controlling influence of faults on earthquakes. The LX borehole is located in the strong earthquake-blank region, which shows relatively weak seismic activities, and the LZX borehole is located close to the intensive earthquake area, in which relatively strong seismic activities occur.

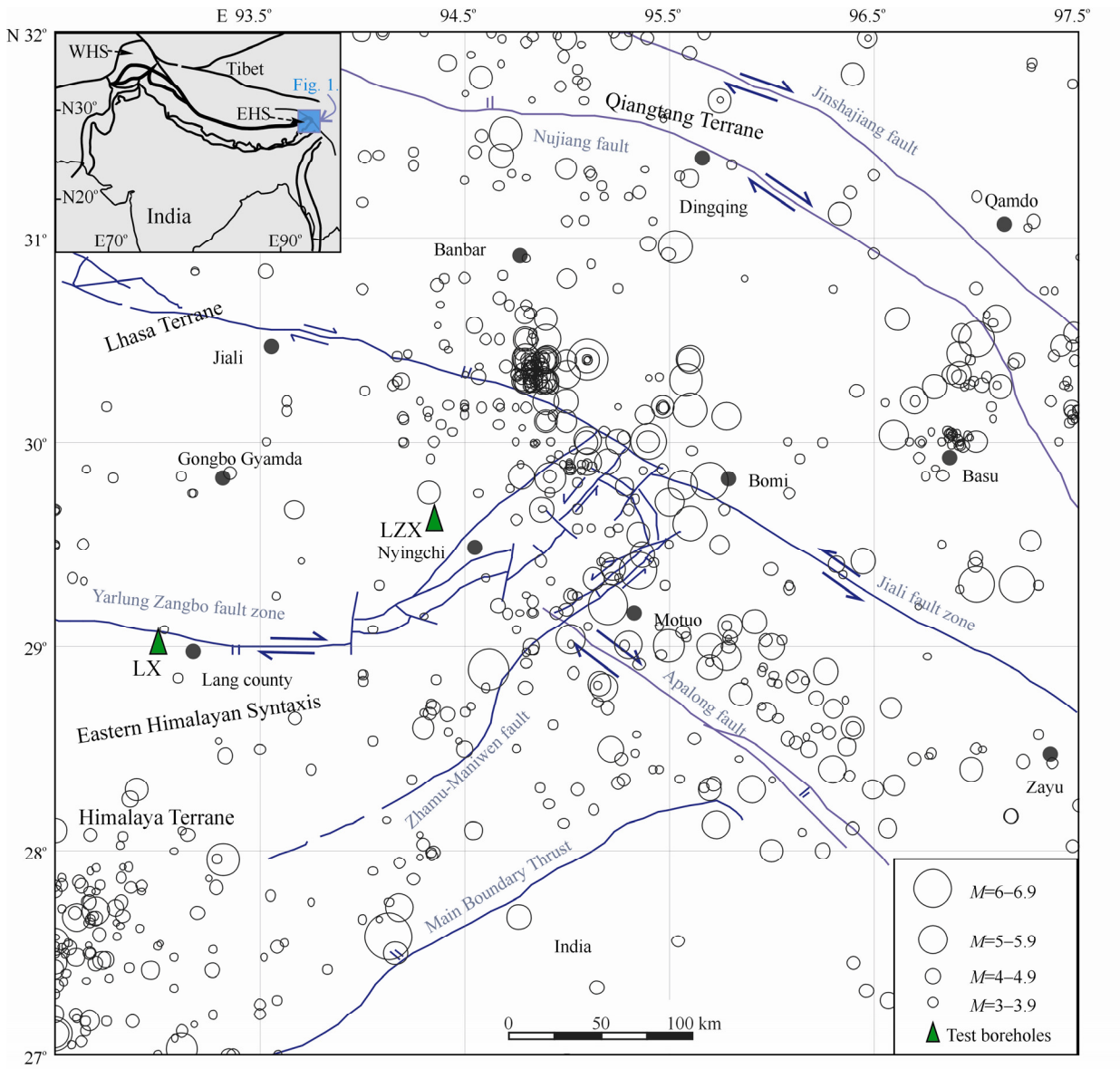

Fig. 1. Simplified tectonic map and seismicity (1970–2013) in the eastern Himalayan syntaxis and the surrounding regions.
EHS, eastern Himalayan syntaxis ; WHS, western Himalayan syntaxis.

3 In Situ Stress Measurement

3.1 Hydraulic fracturing

Hydraulic fracturing is the well-known method for determining the magnitudes and directions of the in situ horizontal principal stress (Hayashi and Haimson, 1991), assuming that the rock mass is linearly elastic, homogeneous, and isotropic. The method is widely used for stress estimates in petroleum industry, engineering projects, and site selection for high-level radioactive waste (Haimson and Cornet, 2003; Zoback, 2007; Zang and Stephansson, 2010; Zhao et al., 2013). Hydraulic fracturing is a straightforward method of obtaining the stress state in the deeper crust because there is no theoretical limit to the depth of measurement.

The apparatus used for the measurements is illustrated in Fig. 2. The measurement requires a sealed segment (i.e., a test interval) of a borehole that is devoid of previous fractures at the measurement depth. The interval is sealed by pressurizing two inflatable rubber packers to a general level of 2–5 MPa such that they can adhere to the borehole wall. The hydraulic fluid, generally water, is pumped into the test interval using an electric pump, gradually increasing the pressure on the borehole wall until a fracture is initiated in the rock. A mechanically controlled transfer valve on the top of the packer is able to switch from packer pressurization to injection into the test interval (Fig. 2a). The flow rate is controlled by a

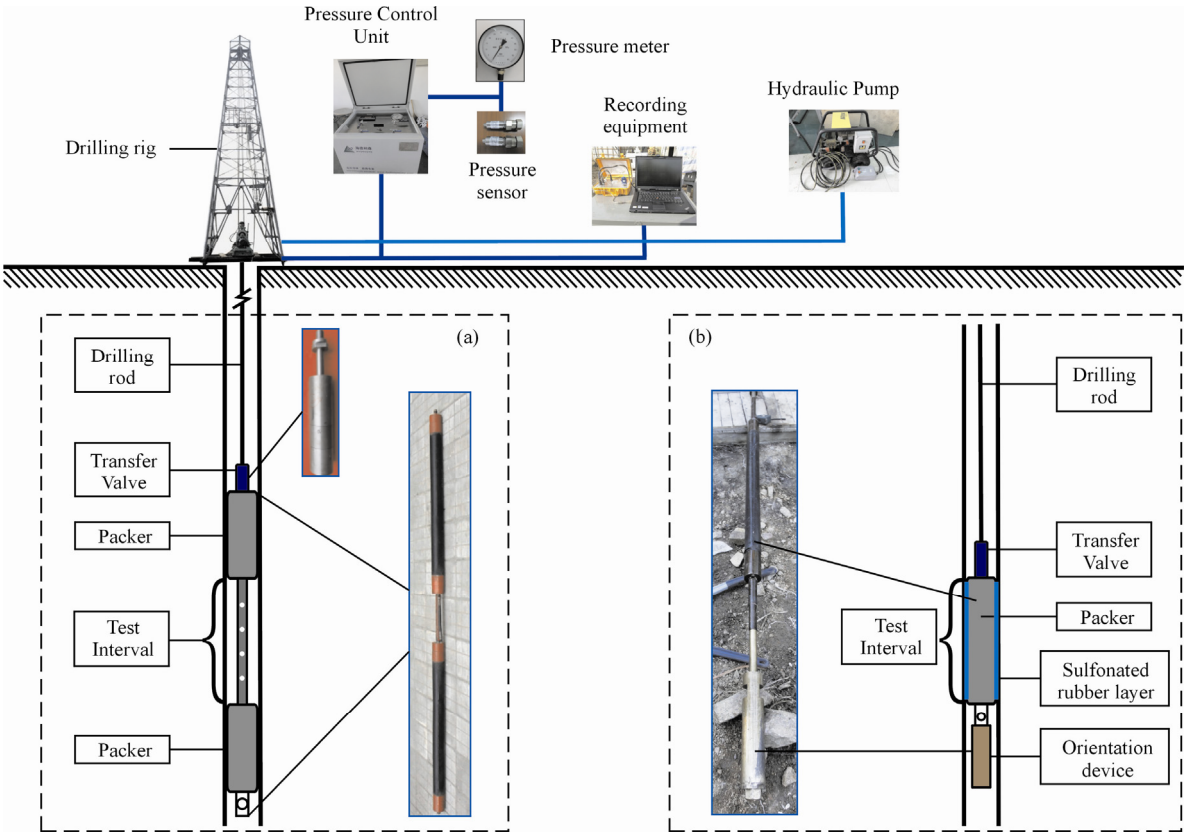

Fig. 2. Schematic illustration of the hydraulic fracturing system.
(a), equipment setup in the hydraulic fracturing test; (b), equipment setup in the impression packer test, which is conducted after the hydraulic fracturing test in the same test interval.

pressure-control unit. A pressure meter is employed to provide real-time information on the hydraulic fluid pressure and a pressure sensor is used to monitor and transmit the pressure data to a recording device. Thus, pressure–time curves are recorded simultaneously. A follow-up re-fracturing test is conducted by injecting water into the test interval again until the previously closed fractures reopen. In this study, the pressurizations in each isolated test interval were repeated for five cycles. The key pressure values used in the computation of the in situ stresses were picked from the pressure–time records, including the breakdown pressure (P_b), instaneous shut-in pressure (P_s), and reopening pressure (P_r).

The principal stress directions are derived from the induced fracture delineation on the borehole wall. Using an impression packer that is covered by a sulfonated rubber layer (Fig. 2b), a distinct geometric copy of the induced fracture can be recorded on the packer surface because of the strong squeeze from the rubber wall into the fracture, as illustrated in Fig. 3. The strike of the fracture traced on the packer is determined by the automatic orientation device. The direction of the maximum horizontal principal stress is perpendicular to that of the minimum horizontal principal stress.

3.2 General conditions of test boreholes

The LZX borehole is located in Nyingchi County, Tibet, China, with water table at 26 m depth. The borehole diameter for hydraulic fracturing measurements was 76 mm at depths ranging from 100 to 300 m. Quaternary loose deposits were drilled to approximately 20 m below the surface, and relatively intact rock masses were extracted deeper down. The lithology was determined to be medium–coarse biotite adamellite using rock photomicrographs (Fig. 4). The LX borehole is located in Lang County, Tibet, China, and was drilled into Paleocene granite. Measurements were performed at depths ranging from 100 to 300 m with a borehole diameter of 91 mm. The general conditions of the two boreholes are summarized in Table 1. Hydraulic fracturing is preferably conducted in elastic and brittle rock with low permeability and porosity, such as granite. The rock types in the LZX

Table 1 General measurement conditions in boreholes LZX and LX

Borehole No.	Borehole depth (m)	Borehole diameter (mm)	Groundwater level (m)	Lithology
LZX	300	76	26	Biotite adamellite
LX	300	91	10	Granite

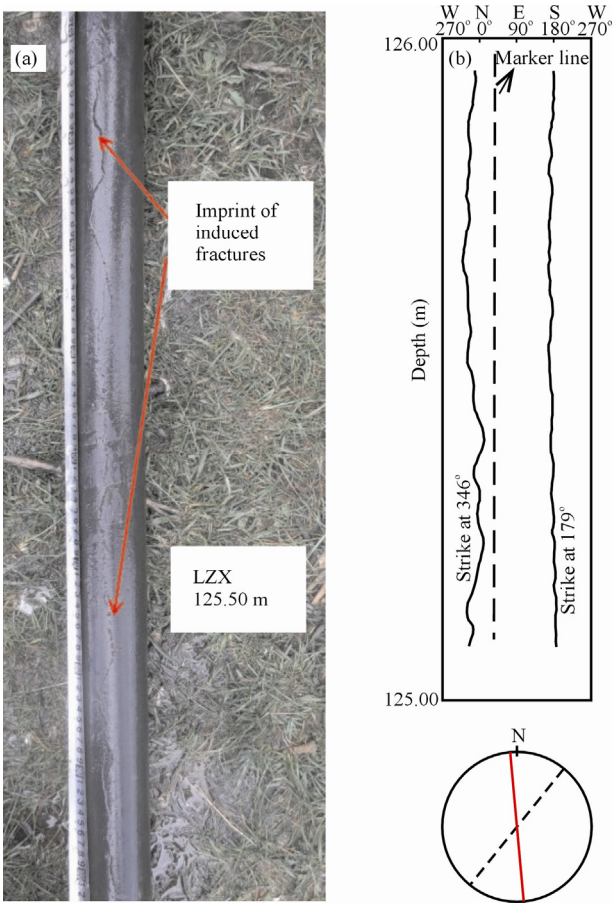

Fig. 3. Typical impression packer test record at the depth of 125.50 m in borehole LZX.
(a), Fracture trace impressed on the packer; (b), Schematic diagram showing hydraulic fracturing traces on the borehole wall and interpreted orientations of the fracture (red solid line)and the marker line (dashed lines).

and LX boreholes are conducive to hydraulic fracturing.

4 Stress Measurement Results

4.1 Stress magnitudes

The maximum and minimum horizontal principal stresses (S_H and S_h, respectively) can be obtained using the correlation formulas given by Eqs. (1) – (2) (Haimson, 1978; Klee et al., 1999; Haimson and Cornet, 2003).

$$S_H = 3P_s - P_r - P_p \quad (1)$$

$$S_h = P_s \quad (2)$$

where the shut-in pressure (P_s) is the pressure reached when the hydraulically induced fracture closes (Haimson and Cornet, 2003), and is often considered as a direct indicator of the minimum horizontal principal stress. The reopening pressure (P_r) is marked as the pressure in a subsequent cycle at which the curve of test interval pressure plotted against time departs from its tangent slope. The pore pressure (P_p) is approximately equal to the hydrostatic pressure in low permeability rocks in the shallow crust (Zoback and Haimson, 1982; Haimson and Doe, 1983; Moos and Zoback, 1990; Barton et al, 1995).

The vertical stress (S_v) is assumed to be equal to the overburden weight per unit area at the test depth, corresponding to the case in which the vertical stress component acts along a principal direction as follows:

$$S_v = \sum_{i=1}^{n} \rho_i g H_i \quad (3)$$

where ρ_i is the mean density of the rock layer i; g is the local gravitational acceleration; H_i is the thickness of layer i; and n is the number of rock layers overlying the test zone (Haimson and Cornet, 2003). In general, a certain value of unit weight of the overlying rock (γ) is used to calculate the vertical stress in the same rock layer with no lithological changes as follows:

$$S_v = \gamma H \quad (4)$$

In the present study, we used 26.5 kN/m^3 as the average unit weight of the overlying rock, referred to the rock mechanics tests conducted in the LZX borehole.

The characteristic hydraulic pressure parameters (shut-in and reopening) used to calculate the in situ stress magnitudes should be derived from the field measurement curves. Thus, the accuracy of the hydro–fracturing stress

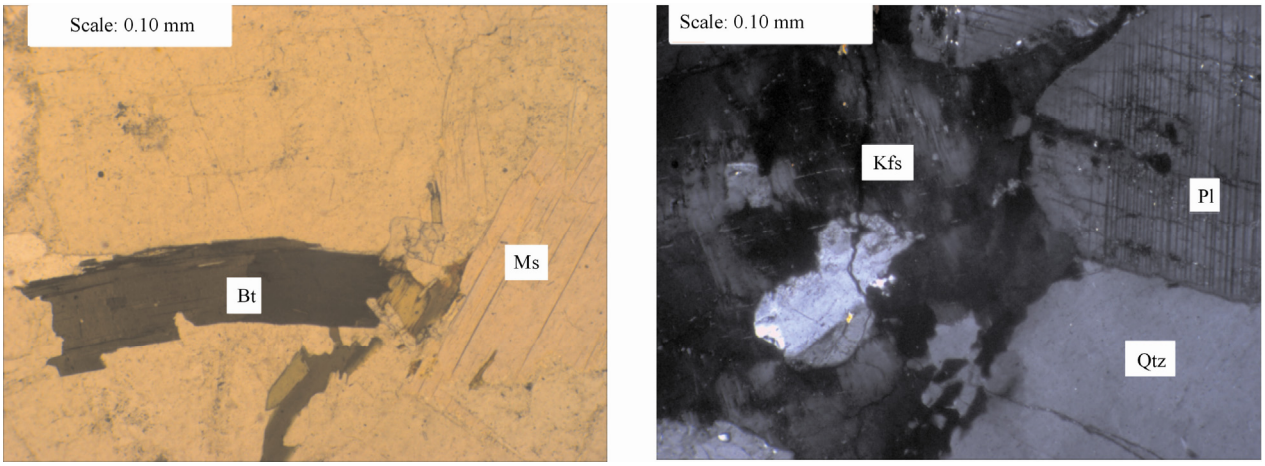

Fig. 4. Rock photomicrographs showing the mineralogical composition of rocks in the LZX borehole.

measurements is strongly dependent on correct interpretation of the pressure–time records obtained during the tests. Typical hydro–fracturing records for the LZX borehole are shown in Fig. 5a, 5b, indicating the clear rock failure process and specific key pressures. In this study, five pressurization cycles were adopted for each test interval, and the last three injection cycles were used to determine the reopening pressure value so that the fractures could be adequately reopened. We used the average value as the final reopening pressure to decrease the error that was determined from a single cycle. As the shut-in pressure is considered to be equal to the minimum horizontal stress for vertical boreholes (Eq. (2)), it is strongly recommended that more than one method be used to obtain the crucial P_s parameter, thus ensuring the reliability of the shut-in pressure value and obtaining good hydraulic fracturing measurement results. The pressure decay rate versus pressure (dP/dt–P) method, the inverted pressure decay rate versus pressure (dt/dP–P) method, and the inflection point method, which are all recommended by the ISRM (Haimson and Cornet, 2003), were adopted and the average values from these three calculations were used to determine the final value of P_s. Fig. 5c shows graphical interpretations of P_s at a measurement depth of 182.30 m in borehole LZX by the three approaches.

On the basis of the relationships between the pressure and time, we successfully obtained the characteristic hydraulic pressure parameters for all the test intervals, and the calculated principal stresses are listed in Table 2. The maximum and minimum horizontal principal stresses in

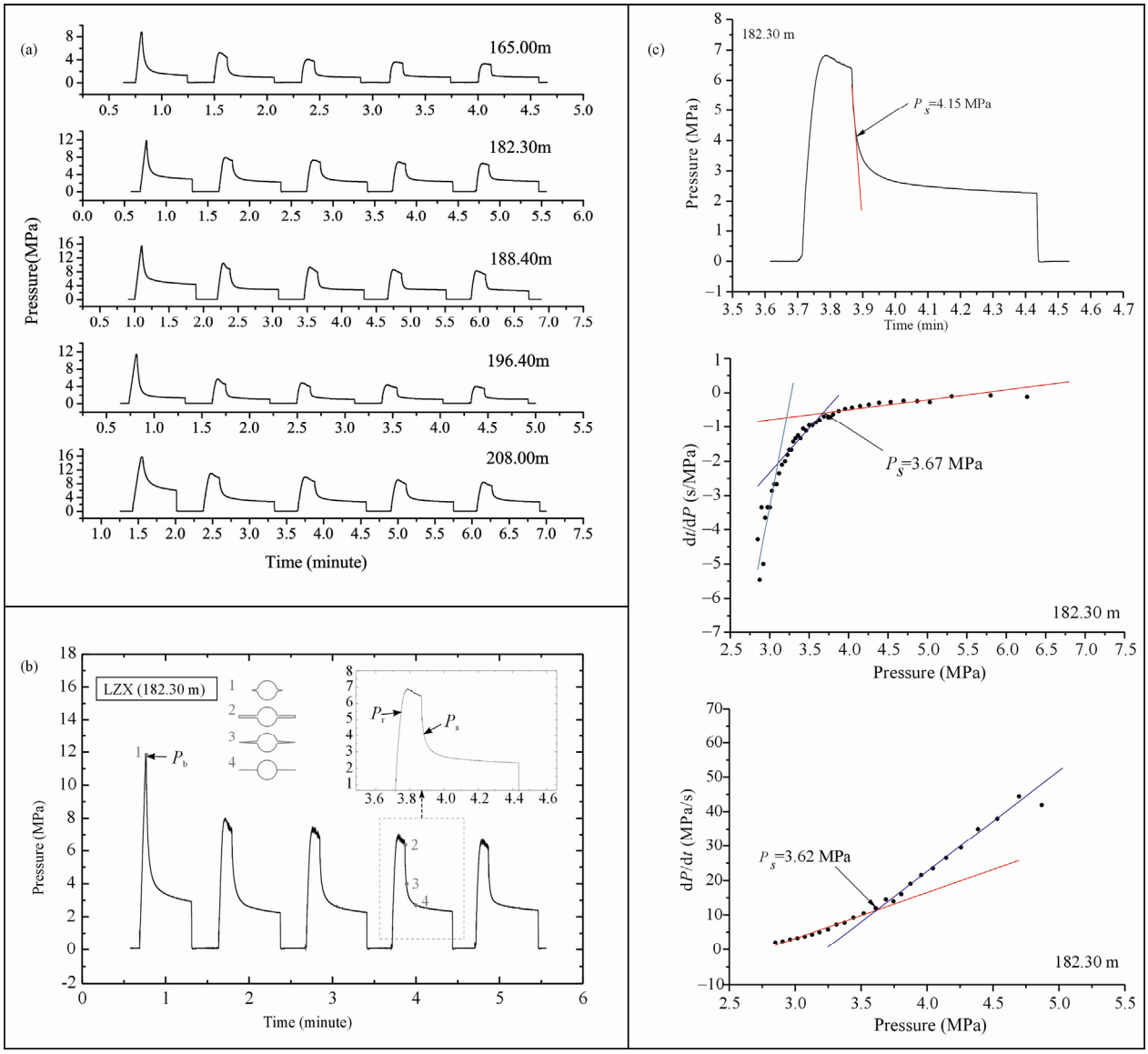

Fig. 5. (a), Typical pressure-time curves of hydraulic fracturing in the LZX borehole; (b), Graph showing the characteristic hydraulic pressure parameters at 182.30 m depth in the LZX borehole; (c), Graphs showing three different methods proposed by the ISRM, the inflection point method, the dt/dP vs. P method, and the dP/dt vs. P method, for determining the shut-in pressure (P_s) at 182.30 m depth in the LZX borehole.

Table 2 Results of hydraulic fracturing stress measurements in boreholes LZX and LX

Borehole	No.	Test interval depth (m)	S_h (MPa)	S_H (MPa)	S_v (MPa)
LZX	1	102.50	2.74	3.74	2.72
	2	115.00	4.18	6.68	3.05
	3	125.50	4.26	6.85	3.33
	4	137.50	3.22	4.73	3.64
	5	149.20	3.66	5.12	3.95
	6	156.00	3.04	4.01	4.13
	7	165.00	3.11	3.92	4.37
	8	182.30	5.63	8.32	4.83
	9	188.40	6.28	8.54	4.99
	10	196.40	3.88	5.24	5.20
	11	208.00	6.44	8.09	5.51
	12	239.53	4.99	7.39	6.35
	13	250.20	7.88	12.62	6.63
	14	288.00	6.15	9.45	7.63
	15	295.93	5.04	7.22	7.84
LX	1	150.40	7.98	13.20	3.99
	2	183.86	9.03	15.16	4.87
	3	222.98	11.15	18.66	5.91
	4	242.90	12.69	20.52	6.44
	5	250.90	13.52	22.29	6.65

borehole LZX are 3.74–12.62 and 2.74–7.88 MPa in the measurement depth range, respectively. In contrast, the two horizontal principal stresses are 13.20–22.29 and 7.98–13.52 MPa in borehole LX, which are 1.5–3.0 times greater than the values for borehole LZX for the same test depths.

Stress magnitude plots for test boreholes are illustrated in Fig. 6. Notes that S_H are generally the maximum principal stresses in the borehole LZX, and the relationship of S_h and S_v is extremely volatile. Low linear dependence of stress magnitudes with depth is also noted. Stresses are much lower in or close to intervals in which fractures were previously developed because of the stress release, and are much higher in intact rock intervals because of stress concentration. For instance, the drill core was extraordinarily intact in the test interval with a center depth of 250.20 m, while was very poor near the test interval (Fig. 7), leading to higher stress magnitude at the test depth of 250.20 m. The measurement results in the LX borehole indicate that the stress state is dominated by horizontal stress, and is characterized by $S_H>S_h>S_v$, S_H and S_h are three and two times higher than S_v, respectively. The stresses, or rather, the horizontal principal stresses in the LX borehole are much higher than in the LZX borehole, and show a gradually increasing trend with increasing depth.

As a result of the influence of faults, the current stress field shows systematic heterogeneity in its orientations and magnitudes (Chang et al., 2010). Earthquakes contribute to stress release, and thus cause a lower-stress environment. Fig. 1 shows the earthquake distribution of the eastern Himalayan syntaxis and surrounding regions: weak seismic activities occur near the LX borehole. The

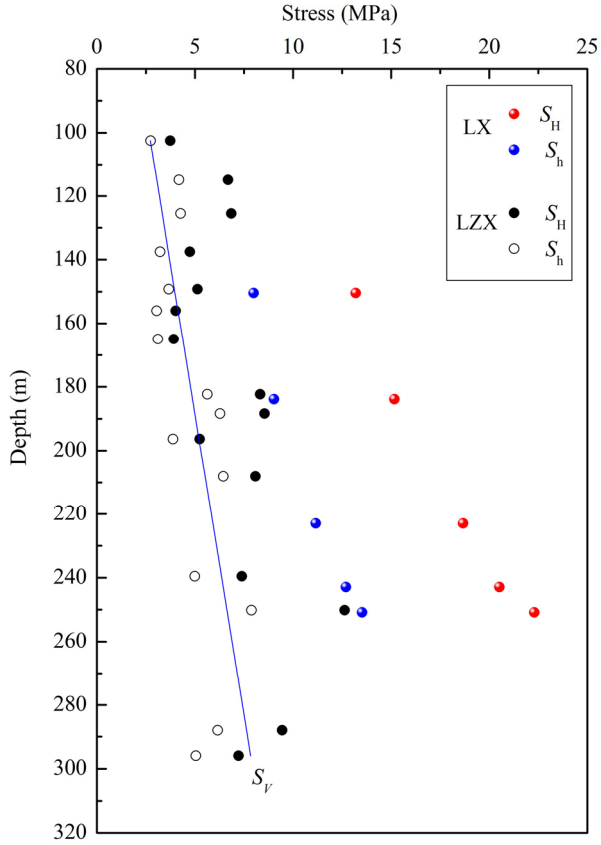

Fig. 6. Variation of the principal stresses with depth.

contemporary fault movement rate is lower around the borehole (Song et al., 2011; Peng and Wang, 2013). Furthermore, the hard and compact granite rock favors stress accumulation, which results in a higher stress field in the LX borehole. In contrast, seismic activities were relatively strong near the LZX borehole and in the surrounding area, contributing to lowering of the stress field in the LZX borehole because of effective stress release. Thus, the stress magnitude appears to be inversely correlated with the density of regional earthquakes and the active fault movement rate.

4.2 Stress orientation

The orientations of the maximum horizontal principal stresses were identified from the borehole impression measurements, and the results are presented in Fig. 8. Two stress direction data in the test intervals with center depths of 150.4 and 183.86 m were obtained in the LX borehole. The results for this borehole indicate that the horizontal stress is almost dominant in the N–S direction. In the LZX borehole, three stress direction data were inferred in the depth range of 120–210 m, in which the directions of the maximum principal stresses in the test intervals with center depths of 125.5, 182.3, and 208 m are N6°W, N31°E, and N21°E.

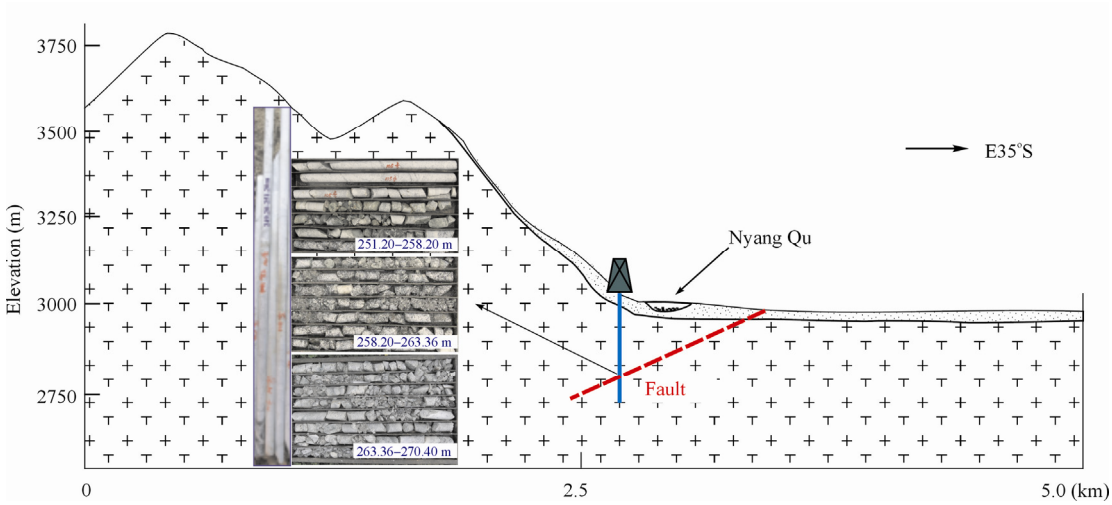

Fig. 7. Geological profile showing the intersection of the LZX borehole and the inferred thrust fault.

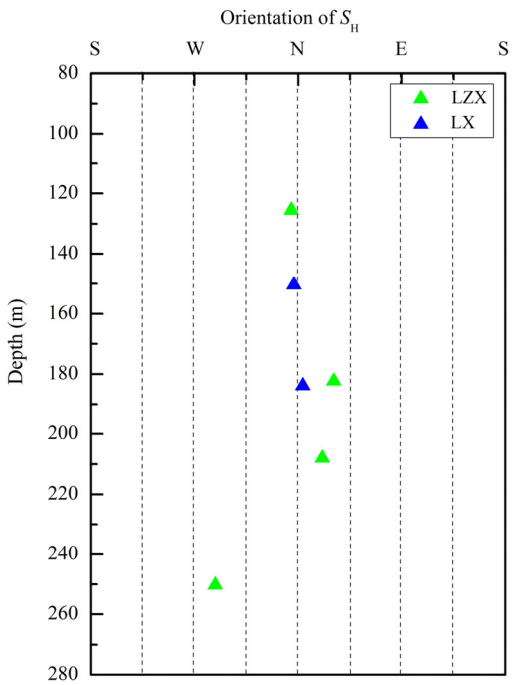

Fig. 8. Variation of the maximum principal stress directions with depth.

Xie et al. (2004, 2015) constructed a contemporary tectonic stress map for China by compiling and interpreting orientation data and divided the tectonic stress field into different districts. In our study, the test boreholes belong to the fourth-order stress district of Motuo–Qamdo (Fig. 9). The orientations of the maximum horizontal principal stresses measured from the LZX and LX boreholes are roughly consistent with the regional stress field. Note that the stress map has a blank zone in terms of the maximum principal orientation, in particular, estimated by field-test methods. As shown in Fig. 9, the inferred stress directions of the background tectonic stress field in the region are almost entirely based on indirect methods such as earthquake focal mechanisms. The present study provides additional stress information for future updates to the crustal stress database of China. Furthermore, the data indicate a relatively uniform stress field throughout the brittle part of the crust, inferred from the consistency between the shallow, near-surface stress orientations and those inferred at depth from earthquake focal mechanisms (Zoback, 1992). It is suggested that measurements obtained at key structural positions, although at shallow depths, are significant for studying the regional crustal stress.

In addition to the above results, the maximum horizontal principal stress orientation at a depth of 250.20 m is dominant in the WNW direction. The stress orientations of the LZX borehole show a transition from the NNE to WNW direction. For a given area, the regional dynamic environment, topography, and geological and tectonic conditions, together control the stress field (Chen et al., 2004). Drill cores indicated that the borehole intersects a fracture zone at a depth of approximately 253 m (see Fig. 7), which may be the main reason for the deviation in stress orientation. As shown in Fig. 11, the LZX borehole is located to the northeast of a NE-striking fault. This fault is inferred to be a thrust fault if it is the same as the fracture exposed in the borehole.

5 Discussions

5.1 Implications of in situ stress for fault activity

Although the process of crustal rupture is extremely complex, it is an important sliding failure resulting from increasing shear stress. Thus, the ratio of the maximum differential stress to the effective mean principal stress, μ_m, is considered to be more correlated with the stress state

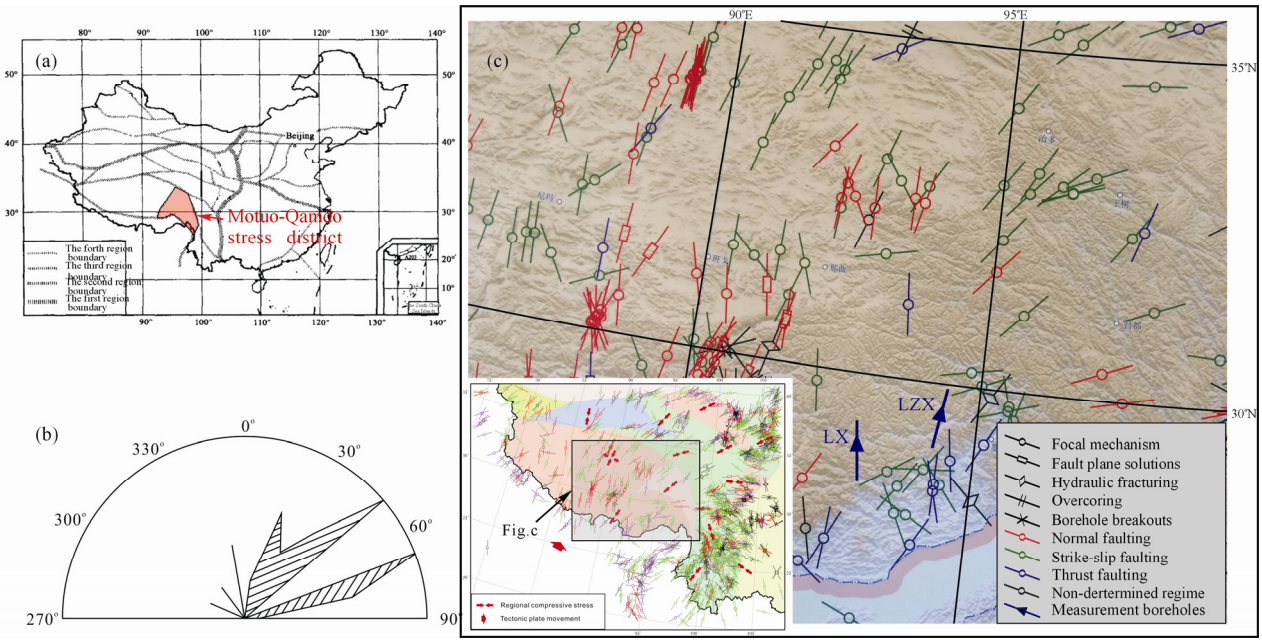

Fig. 9. (a), Recent tectonic stress regions in China; (b), Statistical graph of the maximum principal stress orientations in the fourth order stress district of Motuo–Qamdo; (c), Compressive stress map in test boreholes and surrounding areas. Modified after Xie et al. (2004, 2015).

than the principal stress is to crustal rupture (Tanaka et al., 1998). Townend and Zoback (2000) concluded that the brittle crust in intraplate regions is critically stressed from analysis of deep drilling and induced-seismicity experiments. The value of μ_m is limited because the crust contains critically stressed faults that limit crustal strength. Therefore, μ_m can be used to reveal the regional stress strength and imply fault activity (Wang et al., 2014).

According to the Coulomb frictional-failure criterion, the ratio of the maximum differential stress, $(S_1 - S_3)/2$, to the effective mean principal stress, $(S_1 + S_3)/2 - P_P$, which corresponds to the case in which a critically oriented fault is at the frictional limit, is given as follows (Jaeger and Cook, 1979; Townend and Zoback, 2000; Zoback and Townend, 2001; Wang et al., 2014):

$$\mu_m = \frac{S_1 - S_3}{S_1 + S_3 - 2P_P} = \mu / \sqrt{\mu^2 + 1} \quad (5)$$

where S_1 and S_3 are the maximum and minimum principal stress, respectively (naturally, the intermediate principal stress is marked by S_2) and μ is the frictional coefficient.

The Anderson classification scheme defines three stress states—normal, strike-slip, and reverse—in terms of the corresponding fault nature (Anderson, 1951), which can be used to determine which principal stress, *i.e.*, S_H, S_h, or S_v, corresponds to S_1, S_2, and S_3. For example, the vertical stress, S_v, is the maximum principal stress (S_1) in the normal faulting regimes, the minimum principal stress (S_3) in reverse faulting regimes, and the intermediate principal stress (S_2) in strike-slip regimes.

In the case in which the value of μ_m exceeds that defined by μ on the right-hand side of Eq. (5), the fault will experience frictional sliding along the optimally orientated plane, the normal direction of which makes an angle β with respect to the direction of the maximum principal stress, described as follows:

$$\beta = (\pi/2 + \tan^{-1}\mu)/2 \quad (6)$$

We assume that there are optimally orientated planes that are critically stressed in the current stress state near the LZX and LX boreholes and that the frictional coefficient is 0.6. Considering the in situ measurement results, the potential fault near the LX borehole shows reverse slippage, and is expected to dip at approximately 30° and form a conjugate pair that strikes normal to the direction of S_H, i.e., in the E–W direction. If the potential fault near the LZX borehole slipped simplex, it is expected to be a WNW-striking reverse fault that dips at approximately 30° and forms a conjugate pair, or a sinistral-slip fault that strikes NE or a dextral-slip fault that strikes NW (The orientation of the maximum principal stress in the LZX borehole is estimated to be NNE, excluding the data obtained at the depth of 250.20 m, which is disturbed by a local fault). In fact, many regions around the world show a combination of normal and strike-slip faulting or reverse and strike-slip faulting (Zoback, 2007). Considering the extrusion stress environment and that S_h is approximately equal to S_v ($S_2 \approx S_3$), the potential fault near the LZX borehole is likely to show a combination of reverse and strike-slip faulting.

The upper bounds of μ_m are 0.5–0.7 when the frictional

coefficient is assumed to be in the range of 0.6–1.0 (Byerlee, 1978). Tanaka et al. (1998) conducted repeated stress measurements in two boreholes in southern Hyogo Prefecturefrom 1978 onward, and after the *M* 7.2 South Hyogo earthquake on January 17, 1995, observed the process of stress accumulation and release. There was an increase in μ_m before the earthquake, rising from 0.2 in 1978 to 0.5 near the origin time. After the earthquake, μ_m decreased back to 0.2. Sakaguchi and Yokoyama (2015) observed the same phenomenon before and after the 2011 Tohoku-oki earthquake. The actual values of μ_m might be higher than the known ones because the stress measurement times were 3–6 years prior to the earthquake. Although the earthquake mechanism is extremely complicated, it is critically important and helpful to estimate fault stability by obtaining the actual frictional coefficient for a given fault in different tectonic positions. On the basis of the measurement results obtained by Tanaka et al. (1998) and Sakaguchi and Yokoyama (2015), using 0.5–0.7 as the critical values of μ_m when a fault is critically stressed is reasonable.

The range of values of μ_m is 0.2–0.5, averaged to 0.31 in borehole LZX (see Fig. 10). Note that the values are scattered through the test depth. Because of the inhomogeneity of the rock mass and topographic effects at very shallow depths, stress is generally scattered with depth but converges to a particular value at deeper depths (Yang et al., 2012). The μ_m values in the LZX borehole gradually converge to between 0.3–0.4. The μ_m values in the LX borehole are 0.6–0.65 with an average value of 0.63, exceeding the critical values. As previously described, there are optimally orientated pre-existing faults near the test boreholes LX and LZX. It can be concluded that the optimally orientated fault is likely to be active when the stress buildup is sufficient to destroy the frictional equilibrium. This applies particularly to the LX borehole under the present stress state conditions, and should receive more attention in the future.

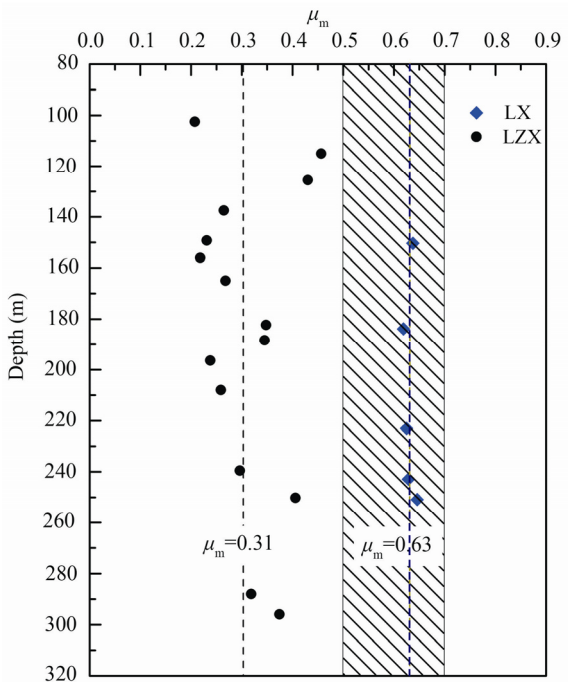

Fig. 10. Plot of the ratio of shear stress to the mean stress vs. depth.
Dashed lines in black and blue represent the average μ_m values of boreholes LZX and LX respectively; Shadow area indicate stronger crust that critically stressed.

5.2 Relationship between the in situ stress field, geological structures, and regional dynamic environment in the Lhasa terrane

The in situ tectonic stress field in the Earth's lithosphere is primarily controlled by tectonic activity. In particular, plate boundary forces that are transmitted into the intraplate regions. As a result, the stress orientations are coupled with the plate active direction and have relative magnitudes that are uniform on a large scale. Furthermore, interactions between intraplate blocks play an important role in the regional uniformity of the in situ stress field (Zoback, 1992; Xie et al., 2004; Heidbach et al., 2010). The contemporary tectonic stress field in China is mainly controlled by movement of the surrounding tectonic plates. In particular, the ongoing power source from continental collision of the India and Eurasia plates is the primary dynamic factor that helps to establish the basic pattern of the present tectonic stress field in Western China. Buoyancy forces derived from lateral variations in the crust and upper mantle structure that support the topography of the Tibetan Plateau dominate the intraplate compressional stress field. In contrast, push and resist forces from the Southern Tibetan Plateau and the Tarim and Alxa blocks lead to the appearance of a shear-stress field in the Northern Tibetan Plateau (Zoback, 1992; Xie et al., 2004). Under this stress background, the compressive stress orientations show a clockwise rotation trend from the Himalayan arc along the Indo–Asian collision zone to the northeastern intra-Tibetan plateau, deviating from approximately N–S to NE–NEE, and to NW in the Sichuan and Yunnan regions (Fig. 9c).

Although the LZX and LX test boreholes are situated in the same stress district (Xie et al., 2004, 2015) and are under the same regional stress background, the measurements results show that there are differences between the two local stress fields. In addition to plate movements and intraplate block interactions, local thermal activity, local structures, and lithology are major factors that disturb the regional stress field. The LX borehole is located near the Yarlung Zangbo fault zone (Fig. 11 F_1),

which is the collision interface between the India and Eurasia plates. The formation age of the Yarlung Zangbo fault zone can be traced back to the plate subduction stage at approximately 90 Ma, and was characterized by shear deformation. As a result of the collision between the northward-moving India plate and the Eurasia plate at approximately 50 Ma, the stress field was dominated by N–S compressional stress (Bai and Yang, 1988; Wu et al., 1990), which is the present stress background. The Gouwu fault (Fig. 11F_2), an early–Middle Pleistocene active fault that strikes approximately N–S for a distance of 18 km, is located east of the LX borehole (Wu et al., 2010). Under the given stress conditions, a fault with dextral characteristics can readily form. The Yarlung Zangbo fault shows dextral slip and extrusion movement since the Late Pleistocene (Tang et al., 2010). However, the movement characteristics differ along the fault: the fault is strongly active to the east of Mainling, and relatively weak to the west of Mainling (Peng and Wang, 2013). Investigation of active faults indicated that the Holocene active N–S-striking Qiangda fault (Fig. 11 F_3) cut through the Yarlung Zangbo fault zone (Wu et al., 2010), which might have divided the eastern Lhasa terrane, resulting in the active difference. The additional stress field that formed as a result of the fault movement in the LX area appears to have a weak influence on the previous stress field on the basis of the measurement results, which is dominated by the N–S stress field. Relative to the LX borehole, the maximum principal stress directions in the LZX borehole deviate from the approximately N–S to NNE, which coincide with the relatively higher movement rate in western section of the Yarlung Zangbo fault. This environment favored formation of a Late Pleistocene active fault, the Lidi fault (Fig. 11 F_4) which has a combination of reverse and strike-slip characteristics. As previously discussed in Section 4.2, the crossed fracture zone in the LZX borehole disturbs the local stress field at the intersection depth, indicating that the maximum horizontal principal stress directions can be significantly affected by local structures.

The measurement results in LX and LZX boreholes reveal that the stress fields are coupled with the geological structures and tectonic active characteristics. We can conclude that large-scale forces related to plate movements and intraplate block interactions determine the appearance of the regional tectonic stress field. The formations of local fault structures are affected by the tectonic stress conditions and, conversely, the additional stress field generated by fault movement overlies the previous stress field to form the contemporary pattern.

6 Conclusions

In situ stress measurements were successfully conducted in boreholes LZX and LX in the Lhasa terrane using the hydraulic fracturing method, revealing the characteristics of the shallow crustal stress state. These results provide additional knowledge for comprehensive understanding of the regional stress field.

(1) The measurement results in both boreholes show that the horizontal principal stresses dominate the stress field, which is the result of horizontal tectonic forces.

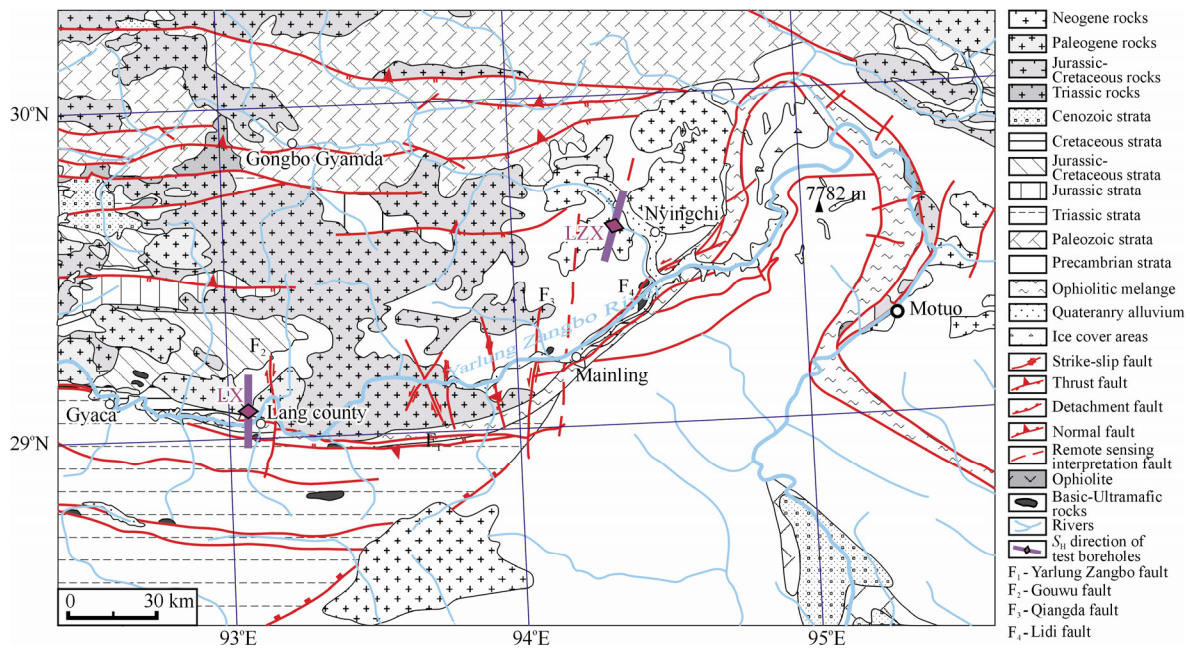

Fig. 11. Geological map of the study area.

Nevertheless, there are differences in both magnitudes and orientations of the stress field between the two boreholes. At the same measurement depths, the magnitudes of the horizontal principal stresses in the LX borehole are 1.5–3.0 times larger than that in the LZX borehole, and show absolutely horizontal principal stress domination. Considering the distributions of earthquakes and faults, the stress magnitude appears to be inversely correlated with the density of regional earthquakes and the active fault movement rate. For the maximum horizontal principal stress direction, measurement results reveal that the stress directions in the LZX borehole rotate from approximately N–S, as in the LX borehole stress field, to NNE. Furthermore, the fracture zone that crosses the LZX borehole disturbs the maximum principal stress at the intersection depth, causing the stress to deviate to the WNW, further demonstrating the influence of local structures on the local stress field.

(2) The ratio of the maximum differential stress to the effective mean principal stress, μ_m, has significant implications for stress strength, and a range of 0.5–0.7 (when the frictional coefficient is assumed to be in the range of 0.6–1.0) is generally regarded as the critical values for a fault being critically stressed. The averaged values of μ_m in boreholes of LZX and LX are 0.31 and 0.63, respectively, from the measurement results. Moreover, there are optimally orientated pre-existing faults near both test boreholes. It can be concluded that an optimally orientated fault is likely to be active when the stress has increased enough to destroy the frictional equilibrium. In particularly, this is applicable to the LX borehole under the present stress state conditions, because the μ_m value exceeds the critical one. It should also be noted that even if μ_m has reached or exceeded the upper bound for fault slippage, this may occur several years or even decades prior to earthquake occurrence (Tanaka et al., 1998; Sakaguchi and Yokoyama, 2015). Although the stress strength in the LZX borehole is relatively weak, the critical values of μ_m for fault slippage will be lower because the friction coefficient is much lower in an actual fault than expected (Boatwright et al., 1996; Carpenter et al., 2009, 2011). At present, the relationship between in situ stress and earthquakes is still under exploratory stage; repeated in situ stress measurements could be a suitable method for use in future studies.

(3) The stress states in boreholes LZX and LX indicate they are in a uniform regional background stress field but diversified local stress fields. Because of its situation in the interaction zone of continental collision between the India and Eurasia plates, formation of the regional stress field in the Lhasa terrane has been mainly affected by compressive forces, and has played a critical role in formation of the subsequent structure. In contrast, the additional stress field generated during local geological evolution has interacted with the previous stress field and yielded a new pattern. The constant interactions of regional dynamic forces, tectonic stress fields and geological structures over geological time led to the appearance of the contemporary stress field.

Acknowledgments

The authors would like to thank professors Chen Qunce and Tan Chengxuan for their beneficial discussions. The excellent collaboration of all participants is highly appreciated. This research was supported by the China Geological Survey Project (No. 12120113038000), the National Science and Technology Major Project (2016ZX05034-003-2) and the scientific research plan of the China Railway Eryuan Engineering Group CO.LTD (No. 13164007).

Manuscript received Sept. 6, 2015
accepted May 6, 2016
edited by Liu Lian

References

Anderson, E.M., 1951. *The dynamics of faulting and Dyke formation with application to Britain*. Oliver and Boyd, Edinburgh.

Bai Jiwen and Yang Jingsui, 1988. Collision of the Indian plate and Eurasian plate and uplift of the Tibetan Plateau. *Regional Geology of China*, 4: 361–368 (in Chinese with English abstract).

Barton, C.A., Zoback, M.D., and Moos, D., 1995. Fluid flow along potentially active faults in crystalline rock. *Geology*, 23: 683–686.

Bilham, R., Gaur, V. K., and Molnar, P., 2001. Himalayan Seismic Hazard, *Science*, 293: 1442–1444.

Boatwright, J., and Cocco, M., 1996. Frictional constraints on crustal faulting. *Journal of Geophysical Research*, 101 (B6): 13895–13909.

Burg, J.P., Nievergelt, P., Oberli, F., Seward, D., Davy, P., Maurin, J.C., Diao, Z., and Meier, M., 1998. The Namche Barwasyntaxis: evidence for exhumation related to compressional crustal folding. *Journal of Asian Earth Sciences*, 16: 239–252.

Byerlee, J.D., 1978. Friction of rocks. *Geophys*, 116 (4/5): 615–626.

Carpenter, B.M., Marone, C., and Saffer, D.M., 2009. Frictional behavior of materials in the 3D SAFOD volume. *Geophysical Research Letters*, 36: L05320.

Carpenter, B.M., Marone, C., and Saffer, D.M., 2011. Weakness of the San Andreas Fault revealed by samples from the active fault zone. *Nature Geoscience*, 4: 251–254.

Chang, C., Lee, J.B., and Kang, T.S., 2010. Interaction between regional stress state and faults, complementary analysis of borehole in situ stress and earthquake focal mechanism in southeastern Korea. *Tectonophysics*, 485: 164–177.

Chen Qunce, Feng Chengjun, Meng Wen, Qin Xianghui and An Qimei, 2012. Analysis of in situ stress measurements at the northeastern section of the Longmenshan fault zone after the 5.12 Wenchuan earthquake. *Chinese Journal of Geophysics*, 55(12), 3923–3932 (in Chinese with English abstract).

Chen Qunce, Mao Jizhen and HouYanhe, 2004. Study on influence of topography on in situ stress by interpretation of measurement data of in situ stress. *Chinese Journal of Rock Mechanics and Engineering*, 23(23): 3990–3995 (in Chinese with English abstract).

Dai Shuang, Zhang Mingzhen, Peng Dongxiang, Wang huawei, Wu Maoxian, Chen Ruiling and Zhang Xiang, 2014. Tectonic and environmental evolutions of the Northern Tibetan Plateau prior to the collision of India with Asia. *Acta Geologica Sinica* (English Edition), 88(2): 425–443.

Deng Qidong, Cheng Shaoping, Ma Ji and Du Peng, 2014. Seismic activities and earthquake potential in the Tibetan Plateau. *Chinese Journal of Geophysics*, 57(7): 2025–2042 (in Chinese with English abstract).

Ding Lin, Zhang Dalai, Yin An, Kapp, P., and Harrison T.M., 2001. Cenozoic structural and metamorphic evolution of the eastern Himalayan syntaxis (Namche Barwa). *Earth and Planetary Science Letters*, 192: 423–438.

Dong Xin, Zhang Zeming, Xiang Hua and He Zhenyu, 2013. Metamorphism and dynamics of the Lhasa terrane, south Tibet. *Acta Geoscientica Sinica*, 34(3): 257–262 (in Chinese with English abstract).

Haimson, B.C., 1978. The hydrofracturing stress measuring method and recent field results. *International Journal of Rock Mechanics and Mining Sciences & Geomechanics Abstracts*, 15: 167–178.

Haimson, B.C., and Cornet, F.H., 2003. ISRM Suggested Methods for rock stress estimation-Part 3, hydraulic fracturing (HF) and/or hydraulic testing of pre-existing fractures (HTPF). *International Journal of Rock Mechanics and Mining Sciences*, 40: 1011–1020.

Haimson, B.C., and Doe, T.W., 1983. State of Stress, permeability, and fractures in the Precambrian Granite of Northern Illinois. *Journal of Geophysical Research*, 88(B9): 7355–7371.

Harris, N., 2007. Channel flow and the Himalayan-Tibetan orogen: a critical review. *Journal of the Geological Society*, 164: 511–523.

Hayashi, K., and Haimson, B.C., 1991. Characteristics of shut-in curves in hydraulic fracturing stress measurements and determination of in situ minimum compressive stress. *Journal of Geophysical Research*, 96(B11): 18311–18321.

He Yulin, Cao Zhongquan, Chen Lichun and Chen Yaming, 2005. Investigation on Site of the 2003 Southern Bomi M_S 5.7 Earthquake, Tibet. *Earthquake Research in China*, 21(4): 469–474 (in Chinese with English abstract).

Heidbach, O., Tingay, M., Barth, A., Reinecker, J., Kurfeβ, D., and Müller, B., 2010. Global crustal stress pattern based on the World Stress Map database release 2008. *Tectonophysics*, 482: 3–15.

Jaeger, J.C., and Cook, N.G.W., 1979. *Fundamentals of Rock Mechanics*. New York, Chapman & Hall.

Klee, G., Rummel, F., and Williams, A., 1999. Hydraulic fracturing stress measurements in Hong Kong. *International Journal of Rock Mechanics and Mining Sciences*, 36: 731–741.

Li Siguang, 1973. *Seismology and Geology*. Beijing, Science Press (in Chinese).

Liu Zhifei, Wang Chengshan and Li Xianghui, 2000. Sedimentary-tectonic evolution of the Yarlung Zangbo suture zone, southern Tibet. *Journal of Tongji University*., 28(5): 537–541 (in Chinese with English abstract).

Meng Wen, Chen Qunce, Du Jianjun, Feng Chengjun, Qin Xianghui and An Qimei, 2012. In-situ stress measurement in Singapore. *Chinese Journal of Geophysics*, 55(8): 2611–2619 (in Chinese with English abstract).

Meng Wen, Chen Qunce, Wu Manlu, Feng Chengjun and Qin Xianghui, 2015.Tectonic stress state changes before and after the Wenchuan M_S 8.0 earthquake in the eastern margin of the Tibetan Plateau. *Acta Geologica Sinica* (English Edition), 89 (1): 801–813.

Moos, D., and Zoback, M.D., 1990. Utilization of observations of well bore failure to constrain the orientation and magnitude of crustal stresses, Application to Continental, Deep Sea Drilling Project, and Ocean Drilling Program Boreholes. *Journal of Geophysical Research*, 95(B6): 9305–9325.

Peng Xiaolong and Wang Daoyong, 2013. Tectonic and active characters of the Yarlung Zangbo fault zone. *Journal of Yangtze University* (Nat Sci Edit), 10(26): 41–44 (in Chinese).

Ren Jinwei, Shen Jun, Cao Zhongquan and Wang Yipeng, 2000. Quaternary faulting of Jiali fault, southeast Tibetan Plateau. *Seismology and Geology*, 22(4): 344–350 (in Chinese with English abstract).

Sakaguchi, K., and Yokoyama, T., 2015. *In-situ stress measurement at shallow depth in the vicinity of the epicenter before and after the 2011 Tohoku-oki earthquake*. ISRM Congress 2015 Proceedings - Int'l Symposium on Rock Mechanics - ISBN: 978-1-926872-25-4.

Song Jian, Tang Fangtou, Deng Zhihui, Cao Zhongquan, Zhou Bin, Xiao Genru, Chen Weitao and Ge Weipeng, 2011. Study on current movement characteristics and numerical simulationof the main faults around Eastern Himalayan Syntaxis. *Chinese Journal of Geophysics*, 54(6): 1536–1548 (in Chinese with English abstract).

Sun Dongsheng, Chen Qunce, Wang Zhongxiu, Zhao Weihua and Li Awei, 2015. In situ stress measurement method and its application in unconventional oil and gas exploration and development. *Acta Geologica Sinica* (English Edition), 89(2): 685–686.

Tan Chengxuan, Hu Qiuyun, Zhang Peng, Feng Chengjun and Qin Xianghui, 2015. Present tectonic stress adjustment process before and after Japan M_W 9.0 earthquake in North and Northeast China and its research significance. *Earth Science Frontiers*, 22(1): 345–359 (in Chinese with English abstract).

Tanaka, Y., Fujimori, K., and Otsuka, S., 1998. In-situ stress measurement and prediction of great earthquake. *Earthquake*, 50(2): 201–208 (in Japanese).

Tang Fangtou, Song Jian, Cao Zhongquan, Deng Zhihui, Wang Min, Xiao Genru and Chen Weitao, 2010. The movement characters of main faults around Eastern Himalayan Syntaxis revealedby the latest GPS data. *Chinese Journal of Geophysics*, 53(9): 2119–2128 (in Chinese with English abstract).

Townend, J., and Zoback, M.D., 2000. How faulting keeps the crust strong. *Geology*, 28: 399–402.

USGS, 2013. *M* 6.6–56 km WSW of Linqiong, China (BETA).

http://comcat.cr.usgs.gov/earthquakes/eventpage/usb000gcdd#summary.

Wang Chenghu, Song Chengke, GuoQiliang, Zhang Yanshan and Ding Jianmin, 2014. Stress build-up in the shallow crust before the Lushan earthquake based on the in-situ stress measurements. *Chinese Journal of Geophysics*, 57(1): 102–114 (in Chinese with English abstract).

Wang, E.Q, Burchfiel, B.C., and Ji, J.Q., 2001. Cenozoic crustal shortening estimation and its geological basis of the eastern Himalayan syntaxis. *Science in China* (Series D), 31(1): 1–9 (in Chinese with English abstract).

Wu Changde, Zhu Hong, Deng zongce and Cui Junwen, 1990. The structural characteristics of Yarlung Zangbo fracture zone. *Bulletin of the Chinese Academy of Geological Sciences*, 21: 87–94 (in Chinese with English abstract).

Wu Manlu, Zhang Yueqiao, Liao Chunting, Chen Qunce, Ma Yinsheng, Wu Jinsheng, Yan Junfeng and Ou Mingyi, 2009. Preliminary results of in-situ stress measurements along the Longmenshan fault zone after the Wenchuan M_S 8.0 earthquake. *Acta Geologica Sinica* (English Edition), 83(4): 746–753.

Wu Zhonghai, Xiong Tanyu, Zhang Yongshuang, Ye Peisheng, Yang Weimin, Yao Xin, Guo Changbao, Hu Daogong, Zhang Chunshan, Liu Jian, Tan Chengxuan and Shi Jusong, 2010. *Active faults survey along the Lhasa-Nyingchi railway line*. Institute of Geomechanics, Chinese Academy of Geological Sciences.

Wu Zhenhan, Yang Yan, Patrick J. Barosh, Wu zhonghai and Zhang Yaoling, 2014. Tectonics and topography of the Tibetan Plateau in Early Miocene. *Acta Geologica Sinica* (English Edition), 88(2): 410–424.

Xie Furen and Cui Xiaofeng, 2015. *Stress map of the recent tectonic stress field in China and adjacent areas*. Beijing: Sino Maps Press.

Xie Furen, Cui Xiaofeng, Zhao Jiantao, Chen Qunce and Li Hong, 2004. Regional division of the recent tectonic stress field in China and adjacent areas. *Chinese Journal of Geophysics*, 47(4): 654–662 (in Chinese with English abstract).

Xu Caijun, 2002. *The kinematic models of crustal movement and tectonic stress field in the Tibetan Plateau*. Beijing: Surveying and Mapping Press (in Chinese).

Xu Jiren and Zhao Zhixin, 2006. Characteristics of the regional stress field and tectonic movement on the Qinghai-Tibet Plateau and in its surrounding areas. *Geology in China*, 33(2): 275–285 (in Chinese with English abstract).

Yang Shuxin, Yao Rui, Cui Xiaofeng, Chen Qunce and Huang Luyuan, 2012. Analysis of characteristics of measured stress in Chinese mainland and its active blocks and North-South seismic belt. *Chinese Journal of Geophysics*, 55(12): 4207–4217 (in Chinese with English abstract).

Yin, A., and Harrison, T.M., 2000. Geologic evolution of the Himalayan Tibetan Orogen. *Annual Review of Earth and Planetary Sciences*, 28: 211–280.

Zang, A., and Stephansson, O., 2010. *Stress field of the earth's crust*. Springer, Heideberg, 208–214.

Zhang Letian, Ye Gaofeng, Jin Sheng, Wei Wenbo, Unsworth Martyn, Jones A.G., Jing Jianen, Dong Hao, Xie Chengliang, Le Pape Florian and Vozar Jan, 2015. Lithospheric electrical structure across the eastern segment of the Altyn Tagh fault on the northern margin of the Tibetan Plateau. *Acta Geologica Sinica* (English Edition), 89(1): 90–104.

Zhao, X.G., Wang, J., Cai, M., Ma, L.K., Zong, Z.H., Wang, X.Y., Su, R., Chen, W.M., Zhao, H.G., Chen, Q.C., An, Q.M., Qin, X.H., Ou, M.Y., and Zhao, J.S., 2013. In-situ stress measurements and regional stress field assessment of the Beishan area, China. *Engineering Geology*, 163: 26–40.

Zhu Shoubiao and Shi Yaolin, 2005.Genetic algorithm-finite element inversion of topographic spreading forces and drag forces of lower crust to upper crust in Tibetan Plateau. *Acta Scientiarum Naturalium Universitatis Pekinensis*, 41(2): 225–234 (in Chinese with English abstract).

Zoback, M.D., 2007. *Reservoir geomechanics*. Cambridge University Press, 130–139.

Zoback, M.D., and Haimson, B.C., 1982. Status of the hydraulic fracturing method for in-situ stress measurements. *The 23rd U. S. Symposium on Rock Mechanics*, 143–156.

Zoback, M.D., and Townend, J., 2001. Implications of hydrostatic pore pressures and high crustal strength for the deformation of intraplate lithosphere. *Tectonophysics*, 336: 19–30.

Zoback, M.L., 1992. First-and second-order patterns of stress in the lithosphere: the world stress map project. *Journal of Geophysical Research*, 97(B8): 11703–11728.

About the first author

MENG Wen, female, born in Shandong province in 1987; master; research assistant of Institute of Geomechanics, Chinese Academy of Geological Sciences; She is now engaged in the in situ stress measurement and tectonic stress field analysis. E-mail: mwen19@sina.com. Phone: 86–010–88815062.